

# Calibrating Milky Way dust extinction using cosmological sources

Edvard Mörtzell<sup>1</sup>

<sup>1</sup> The Oskar Klein Centre for Cosmoparticle Physics, Department of Physics,  
Stockholm University, AlbaNova University Center, S-106 91 Stockholm, Sweden

E-mail: edvard@fysik.su.se

**Abstract.** By investigating the correlations between dust column density as inferred from infrared data and the observed colours of celestial objects at cosmological distances with small colour dispersion, we constrain the properties of Milky Way dust. Results derived using colours of quasars, brightest central galaxies and large red galaxies are broadly consistent, indicating a proportionality constant between the reddening  $E(B - V) \equiv A_B - A_V$  and the dust column density  $D^T$  (given in units of MJy/sr) of  $p = E(B - V)/D^T \sim 0.02$  and a reddening parameter  $R_V \equiv A_V/E(B - V) \sim 3$  with fractional uncertainties of the order 10 %. The data does not provide any evidence for spatial variations in the dust properties, except for a possible hint of scatter in the dust extinction properties at the longest optical wavelengths.

## 1. Introduction

Astronomical data need to be corrected for extinction from dust in the Milky Way. Typical (albeit with large variations) values for the reddening  $E(B - V) \equiv A_B - A_V$  is 0.02 with  $A_V \sim 0.06$ , see Fig. 1. ‡ In this paper, we reinvestigate the relation between the Milky Way reddening and the dust maps generated in Schlegel et al. [12], using colours of quasars (QSOs) observed within the Sloan Digital Sky Survey (SDSS). We also compare with results from SDSS observations of Brightest Central Galaxies (BCGs) and Luminous Red Galaxies (LRGs). Compared with the original investigation in Schlegel et al. [12], the improved statistics and multiple band photometry potentially allow us to decrease the errors on a linear relation while simultaneously constraining the properties of Milky Way dust, in this case the total to selective extinction ratio  $R_V \equiv A_V/E(B - V)$ .

We also perform a simple check to investigate if there are deviations from the linear relation in that regions with high dust column density have more or less reddening than the linear prediction. No such effect is found. Neither do we find any firm evidence of scatter in the dust properties as a function of the line-of-sight.

‡ The dust maps of Schlegel et al. [12] with degree resolution peak at  $E(B - V) \sim 0.016$  mag, with a mean value of 0.048 mag, and a median value of 0.028 mag.

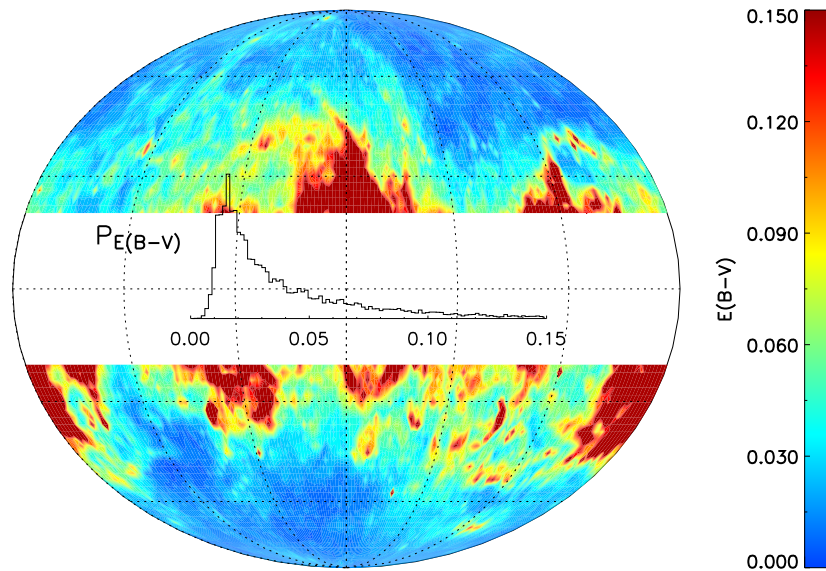


**Figure 1.** Galactic dust extinction represented as  $E(B-V)$  with degree resolution for galactic latitudes  $|b| > 20^\circ$ , together with the corresponding probability distribution function. Data taken from Schlegel et al. [12].

While noting that there is still room for non-linear behaviour as well as scatter in dust properties at angular positions and scales not probed by the data, we conclude that at the positions and scales studied in this paper, it is a fair assumption that the reddening is linear to the dust column density  $D^T$  (in units of MJy/sr) with proportionality constant  $p = E(B-V)/D^T \sim 0.02$  and  $R_V \sim 3$ . The relative errors are of the order of 10% and are mainly limited by uncertainties in the filter response functions and the source spectral templates.

This agrees well with the results of Berry et al. [1] where SDSS photometry of 73 million stars is used to obtain the dust extinction towards each star giving a three-dimensional dust map of the Milky Way in the direction of the observed stripes. The results from this analysis are consistent with  $R_V = 3.0$ , with a statistical and systematic error of 0.1 and a scatter of 0.2.

In Peek and Graves [10], the colours of passively evolving galaxies from the SDSS are used to obtain corrections to the results of Schlegel et al. [12]. They find that the reddening in regions of low dust temperature are underpredicted with maximum deviations in  $E(B-V)$  of 45 millimagnitudes.

In the following, all limits are given as 95.4% confidence levels (CL) corresponding to  $\chi^2 = \chi^2_{\min} + 3.98$  for one parameter and  $\chi^2 = \chi^2_{\min} + 6.16$  for two parameters.

## 2. Method

We use the temperature corrected dust maps from Schlegel et al. [12] to derive a reddening map by correlating the dust maps to the observed colours of celestial objects,

preferably with a small intrinsic colour dispersion. The dust map, given as the dust column density  $D^T$  in units of MJy/sr, is derived from COBE/DIRBE data allowing for a resolution of approximately one degree. We note that in Kohyama et al. [6], IRAS data is used to reach a resolution of five arc minutes in the Cygnus region. However, no all sky map data is available for these data.

As a first attempt, we assume that the observed colour, e.g.  $E(B - V)$ , is proportional to the dust column density

$$E(B - V) = pD^T + m, \quad (1)$$

where we set out to derive the proportionality constant  $p$ , and  $m$  represents an arbitrary offset that is marginalised over (possibly due to, e.g., calibration errors giving the wrong mean colour) and the dust column density is given in units of MJy/sr, making  $p$  dimensionless. In Schlegel et al. [12], a value of the reddening parameter  $R_V = 3.1$  was assumed, yielding a value of the proportionality constant  $p = 0.0184 \pm 0.0014$  for Mg2-calibrated BCGs.

Note that this can in principle be done for any set of filters,  $X$  and  $Y$ ,

$$E(X - Y) = k_{XY}D^T + m_{XY}, \quad (2)$$

and that multiple colour data thus can be used to infer dust properties.

### 2.1. Fitting for $R_V$ and $p$

Since SDSS data allow for multiple colour combinations, we are able to fit also for the properties of the Milky Way dust and relax any prior assumptions on the reddening parameter  $R_V$ . The SDSS  $[u, g, r, i, z]$  filters have central wavelengths at  $[3543, 4770, 6231, 7625, 9134]$  Å and we thus expect  $g - r$  and/or  $u - r$  to correspond closest to  $B - V$ .

For each source and filter, we calculate the transmitted flux using a redshifted source template. This is done for a grid of dust models in order to compute how each dust model will affect a given colour. Note that in doing this, we need to calculate the transmitted flux for each dust model separately since  $k$ -corrections will depend on the dust model. In practice, we have created tables that list the necessary  $k$ -corrections over a grid of redshifts,  $A_V$  and  $R_V$  for each filter that we interpolate between.

After calculating how a given dust model affects each source template in each filter, we can compare with the actual observed colours,  $E(X - Y)$ , allowing us to constrain the parameters  $p$  and  $R_V$ .

Normalizing such that zero column density corresponds to zero reddening, i.e.  $m = 0$  in Eq. 1, defining  $f(\lambda) \equiv A(\lambda)/A_V$  and using

$$A_V = pR_V D^T, \quad (3)$$

we can write

$$\frac{A_1 - A_2}{D^T} \equiv \frac{\Delta m}{D^T} = pR_V(f_1 - f_2), \quad (4)$$

and

$$d\left(\frac{\Delta m}{D^T}\right) = dpR_V(f_1 - f_2) + pdR_V(f_1 - f_2) + pR_V d(f_1 - f_2), \quad (5)$$

showing how uncertainties in  $D^T$ ,  $\Delta m$  and the dust extinction curve  $f(\lambda)$  translates into uncertainties in  $p$  and  $R_V$ . In the following, we will make use of the Milky Way extinction curves  $f(\lambda)$  as parametrised in Cardelli et al. [2] (CCM) and Fitzpatrick [4] (FTZ), plotted in Fig. 3 together with the (arbitrary normalised) SDSS filter transmission curves.

We now turn to the expected degeneracy between  $R_V$  and  $p$  and how this can be broken using multiple colour data. In the CCM-model, we have  $f = a + b/R_V$  and  $f_1 - f_2 = (a_1 - a_2) + (b_1 - b_2)/R_V \equiv \Delta a + \Delta b/R_V$ . Setting  $d(\Delta m/D^T) = 0$  in Eq. 5 and putting  $d(\Delta a) = d(\Delta b) = 0$ , i.e. no systematic error in the extinction curves, we obtain

$$\frac{dp}{p} = \frac{-dR_V}{R_V + \Delta b/\Delta a}. \quad (6)$$

This can be integrated to give

$$p = p_0 \frac{R_{V,0} + \Delta b/\Delta a}{R_V + \Delta b/\Delta a}, \quad (7)$$

describing the relation between different values of  $R_V$  and  $p$  giving the same extinction per unit column density  $\Delta m/D^T$ . The degeneracy lines for the SDSS standard colours  $u - g$  (dark red),  $g - r$  (red),  $r - i$  (orange) and  $i - z$  (yellow) are plotted in Fig. 2, displaying the power of multiple colour data to break the degeneracy between  $p$  and  $R_V$ . We see that  $p$  is anti-correlated with  $R_V$ , if the difference  $(A_X - A_Y)/A_V$  is decreasing slower than  $1/R_V$  with  $R_V$ , which is the case for the three reddest SDSS standard colours. The slope of these curves compare well with the confidence contours derived from data in the forthcoming sections.

### 3. Error analysis

We first note that constant filter calibration errors do not affect our results, since we are marginalising over any constant offset between the observed and theoretically calculated colours. However, we may get systematic effects if the spectral template is wrong and/or if the shape of filter response function is incorrectly modeled since this will change the effective wavelength of the filters. We assume that this will induce fractional uncertainties in the effective wavelengths of  $[0.02, 0.01, 0.01, 0.01, 0.01]$  in  $[u, g, r, i, z]$  filters [3]. We note that this error will be a true systematic since the effect will be correlated between all source redshifts and colours. For comparison, for our QSO template, effective wavelengths will vary with  $\sim 2 - 3\%$  when varying the source redshift and dust parameters. Moreover, we assume a fractional error of 10% in the dust map values  $D^T$ . §

§ A possible caveat not taken into account in this paper is that the dust map may be contaminated by the extragalactic background at low values (B. Menard, private communication).

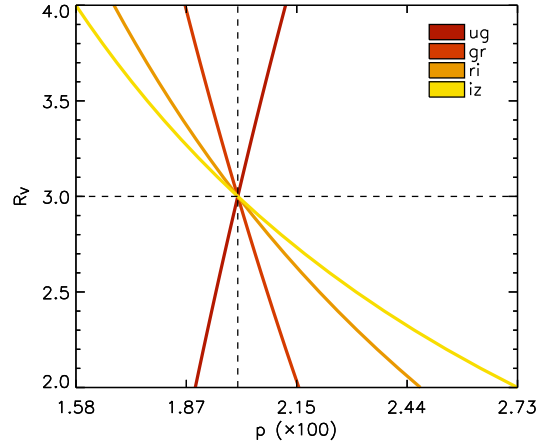


**Figure 2.** Degeneracy between parameters  $p$  and  $R_V$  for SDSS colours  $u - g$  (dark red),  $g - r$  (red),  $r - i$  (orange) and  $i - z$  (yellow). The degeneracy lines correspond to a reddening equal to that of having  $p = 0.02$  and  $R_V = 3.0$ . It is evident that multiple colours allow the degeneracy to be broken.

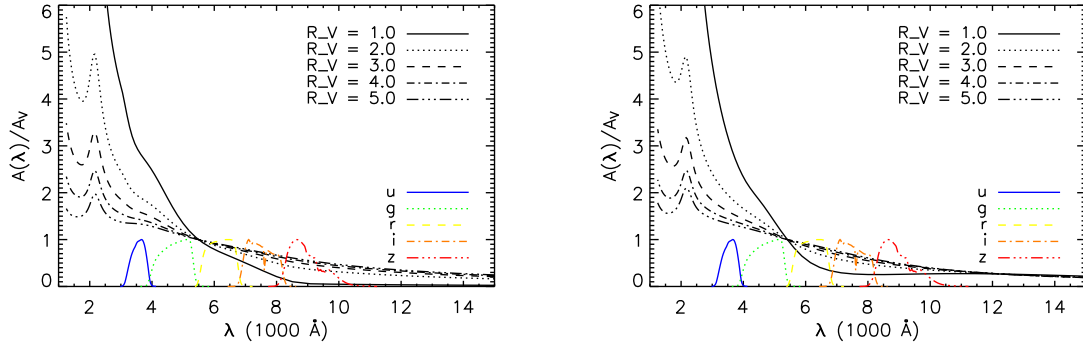


**Figure 3.** Dust extinction curves for different values of  $R_V$  shown together with the (arbitrary normalised) SDSS filter transmission curves. *Left:* Extinction curve for the CCM parametrisation. *Right:* Extinction curve for the Fitzpatrick parametrisation.

We incorporate uncertainties using a Monte Carlo based approach as follows:

- Pick a random value for the shift in effective wavelength for each filter and compute the corresponding colour offset. Also randomise the value for  $D^T$  at each sky position within the given uncertainties.
- Derive the likelihood over a grid of fitted parameters. In doing this, use the statistical sources of error from observational uncertainties and the intrinsic colour dispersion of the sources.
- Repeat  $N$  times (we have used  $N \sim 50$ ) to obtain  $N$  likelihood functions.
- Compute the mean of the  $N$  likelihood functions.

In this way, we take full account of the different correlations between sources of error, and

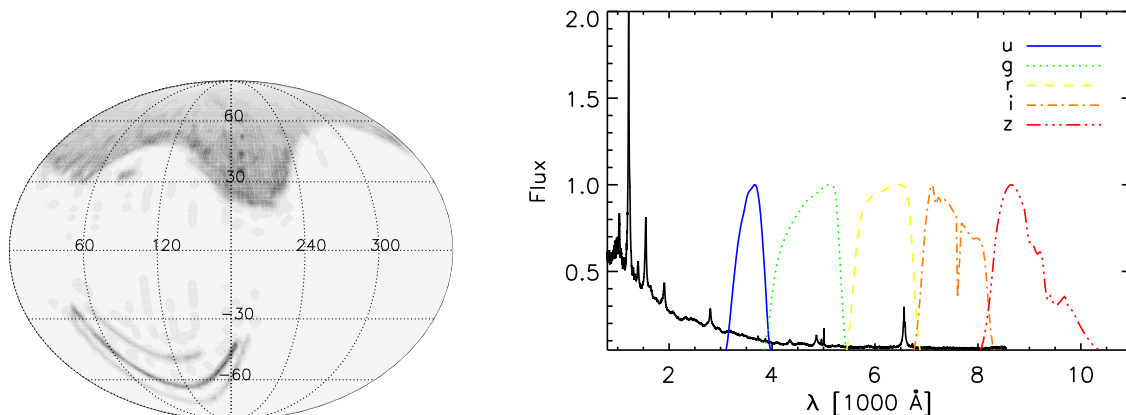


**Figure 4.** *Left:* Angular positions of the SDSS QSOs used in this analysis with darker colours corresponding to higher observed surface densities of QSOs, reflecting the given survey strategy. *Right:* Restframe QSO template spectrum shown together with arbitrary normalised SDSS filter transmission curves.

the resulting confidence contours correctly incorporates both statistical and systematic effects. As noted in Sec. 1, the dominating source of error is the possibility of shifts in the effective filter wavelengths, originating in uncertainties in the filter response functions and the source spectral templates.

#### 4. Quasar analysis

It is well known that QSOs form a relatively homogeneous group of objects in terms of colours and spectral features. They also have large flux at short wavelengths which means that we can use blue colours, e.g.,  $u - r$  also for high redshift sources, allowing us to effectively break the degeneracy between  $p$  and  $R_V$  as shown in Fig. 2. We use the fifth edition of the Sloan Digital Sky Survey (SDSS) Quasar Catalog [13] consisting of 77 429 objects. The area covered by the catalogue is 5 740 deg<sup>2</sup>, see Fig. 4.

QSOs have also been used successfully to constrain the amount and properties of dust in galaxies at cosmological distances [7, 8] and for intergalactic dust [9].

Since we are primarily interested in the colours of QSOs, it is important to understand how the objects in the SDSS QSO catalogue are selected in order to assess whether there are selection effects that need to be taken into account. The QSO candidate selection is based on the position of sources in multidimensional SDSS colour space. In terms of colours, QSOs are identified as being outside the four-dimensional stellar loci points in  $[u, g, r, i, z]$  space [11] plus a number of extra inclusion and exclusion regions. Since the selection is made after correcting for the extinction maps in Schlegel et al. [12], assuming that these provide a fair model for the extinction, there is no reason that the selection should be severely affected by Milky Way dust extinction.

Only QSOs in the redshift range  $0.5 < z < 3.0$  are considered, as QSOs outside this

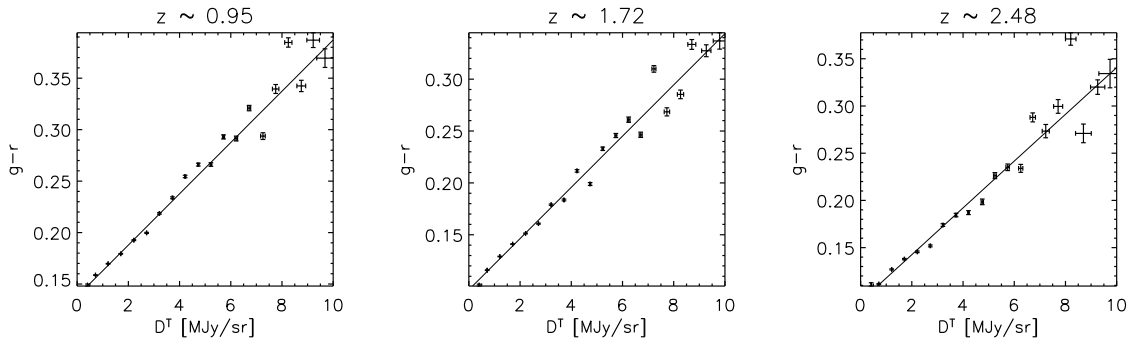


**Figure 5.** Observed  $g - r$  colour as a function of galactic dust column density for SDSS QSOs at three different redshifts. Note the close to, but not perfectly, linear relationship between the observed colour and the dust density.

range are less accurately described by the spectral template used, created by combining the HST radio-quiet composite spectrum [14] with the SDSS median composite spectrum [15] as described in Östman et al. [7, 8]. Generally, all colours are relatively homogeneous at  $z \lesssim 2$ . Typically, at  $z \sim 1$ , we have  $\sigma(u - g) = 0.15$ ,  $\sigma(g - r) = 0.13$ ,  $\sigma(r - i) = 0.093$  and  $\sigma(i - z) = 0.11$ . However, when the Lyman- $\alpha$  emission is being redshifted into the observed filters, the dispersion increases. We thus cut the  $u$ -band data at  $z > 3000/1210 - 1 \sim 1.5$  and the  $g$ -band data at  $z > 4000/1210 - 1 \sim 2.3$ .

In order to display the close to linear relationship between the observed QSO colour and the dust density, in Fig. 5 we show the observed QSO  $g - r$  colour as a function of galactic dust column density at redshifts  $z \sim 0.95$ ,  $z \sim 1.72$  and  $z \sim 2.48$ .

Results for the full fit of  $p$  and  $R_V$  are shown in Fig. 6 for the CCM dust extinction parametrisation (left panel) and the Fitzpatrick parametrisation (right panel). Solid colours correspond 95.4% C.L. for two parameters. Our constraints are  $p = 0.0205 \pm 0.0015$  and  $R_V = 3.10 \pm 0.43$  (CCM) and  $p = 0.0190 \pm 0.0015$  and  $R_V = 3.25 \pm 0.37$  (FTZ) (95.4% C.L. for one parameter). Although consistent at the 95.4% C.L., compared to the  $r - i$  and  $i - z$  colours, we have on average less extinction in  $u - g$  and more extinction in  $g - r$  for the CCM parametrisation. For Fitzpatrick dust, compared to  $g - r$  and  $r - i$ ,  $u - g$  has less extinction and  $i - z$  more extinction on average.

Albeit with very limited resolution, multiple colour data allow us to also derive the dust extinction curve directly from the data, without the need to assume any specific dust extinction parametrisation. For each colour, we fit the slope,  $k_{XY}$ , in Eq. 2, apply the necessary  $k$ -corrections and normalise the extinction to be zero in the  $V$ -band. In Fig. 7, we show the dust law as derived from QSO colours compared to the extinction curves for some fiducial dust models. Assuming the errors to be accurately represented by the uncertainty of the slope in the linear fit, the error bars are too small to be visible. However, this assumption is valid only in the case that the relation between the reddening and the dust column density indeed is linear and constant over the field. Also,

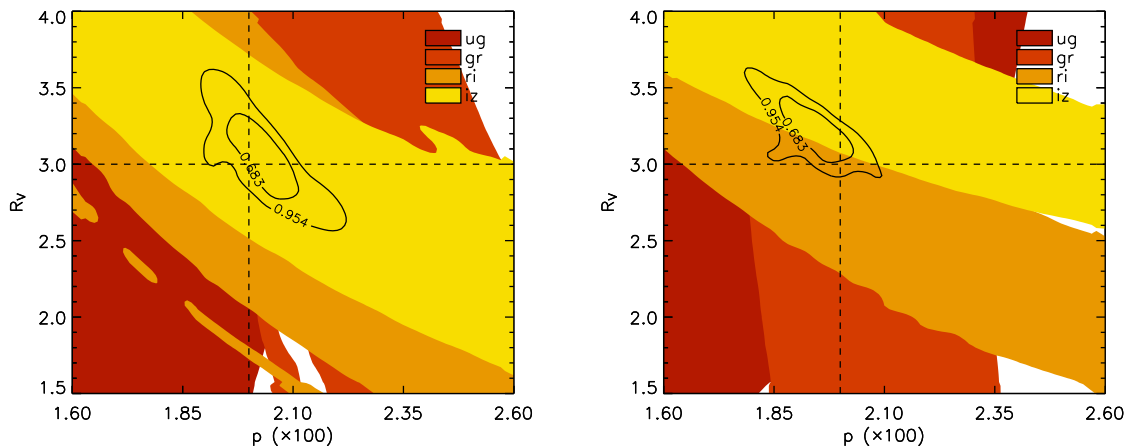


**Figure 6.** Constraints on  $p$  and  $R_V$  as derived from the observed colours of SDSS QSOs and the measured dust column density at the angular position of each QSO. Solid colours correspond 95.4% C.L. for two parameters. *Left:* Results for CCM dust corresponding to 95.4% C.L. for one parameter of  $p = 0.0205 \pm 0.0015$  and  $R_V = 3.10 \pm 0.43$ . *Right:* Results for Fitzpatrick dust corresponding to 95.4% C.L. for one parameter of  $p = 0.0190 \pm 0.0015$  and  $R_V = 3.25 \pm 0.37$ .

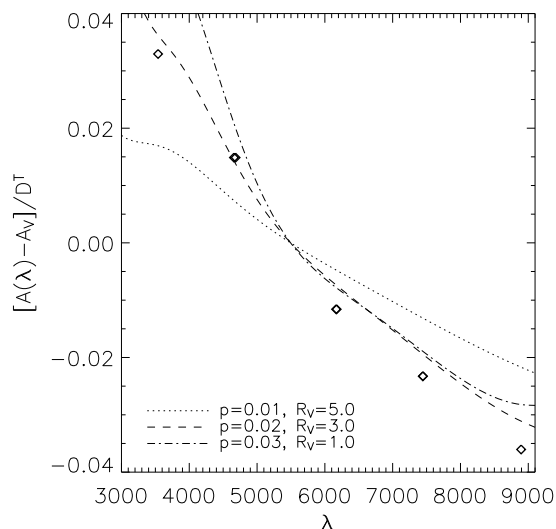


**Figure 7.** Empirical dust law as derived from QSO colours (diamonds) compared to the extinction curves of CCM dust with  $p = 0.01, R_V = 5.0$  (dotted curve),  $p = 0.02, R_V = 3.0$  (dashed curve) and  $p = 0.03, R_V = 1.0$  (dash-dotted curve).

the dominating source of error of possible systematic shifts in the effective central filter wavelengths have not been included. Note that since the normalisation is arbitrary, only the shape of the derived extinction curve is relevant.



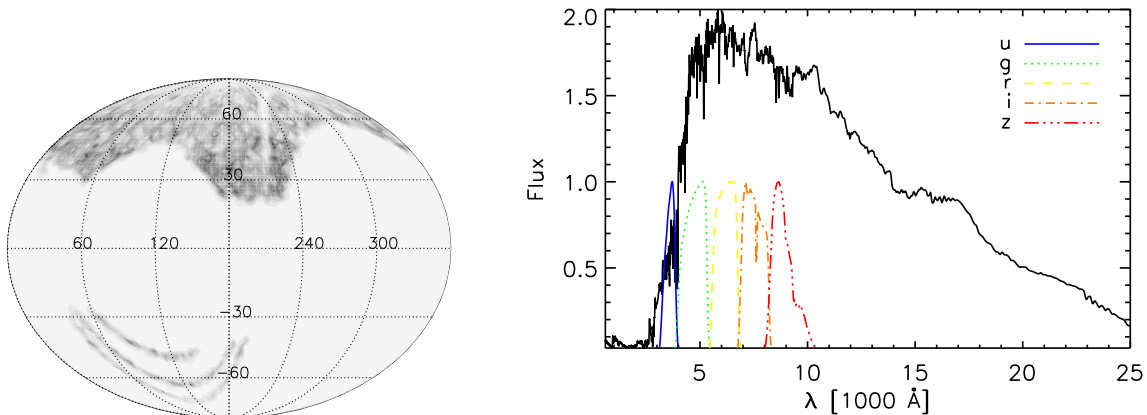


**Figure 8.** *Left:* Angular positions of the SDSS BCGs used in this analysis with darker colours corresponding to higher observed surface densities of BCGs. *Right:* Restframe BCG template spectrum shown together with arbitrary normalised SDSS filter transmission curves. Note that the same template is used for the LRG analysis.

## 5. Brightest Central Galaxies analysis

The brightest galaxies at the centre of galaxy clusters are empirically known to be relatively homogeneous in colour. Since high luminosity early type galaxies are generally redder than low luminosity ones (usually attributed to higher metallicity), the colour dispersion can be further reduced using colour-magnitude relations. However, in this paper, we defer from employing any such calibration.

We have used data from the MaxBCG catalogue of 13 823 galaxy clusters from the Sloan Digital Sky Survey [5]. In order to extract the full photometric data for the brightest central galaxies (BCGs), we retrieved all objects within 6 arc sec from the BCG positions. We managed to identify and retrieve  $[u, g, r, i, z]$  data for 13 796 BCGs with redshifts  $0.046 < z < 0.37$ . The angular positions of the BCGs are depicted in Fig. 8. Generally, all colours involving the  $u$ -band are not very well-determined. Typically (at  $z \sim 0.2$ ), we have  $\sigma(u-g) = 0.32$ ,  $\sigma(g-r) = 0.059$ ,  $\sigma(r-i) = 0.029$  and  $\sigma(i-z) = 0.042$ .

We cut all colours involving the  $u$ -band at  $z > 0.15$  since the colour dispersion becomes very large at those redshifts. Results for fitting  $p$  and  $R_V$  to the BCG data are shown in Fig. 9. Our constraints are  $p = 0.0205 \pm 0.0030$  and  $R_V = 2.89 \pm 0.88$  (CCM) and  $p = 0.0177 \pm 0.0020$  and  $R_V = 3.42 \pm 0.48$  (FTZ) (95.4 % C.L. for one parameter). Similar to the QSO constraints, compared to  $r-i$  and  $i-z$  that gives  $p = 0.02$  for  $R_V = 3$ , we have less extinction in  $u-g$  and more extinction in  $g-r$  for the CCM parametrisation. For Fitzpatrick dust,  $g-r$  and  $r-i$  gives  $p = 0.02$  at  $R_V = 3$  while  $u-g$  has less extinction and  $i-z$  more extinction. In Fig. 10, we show the empirically derived dust law.

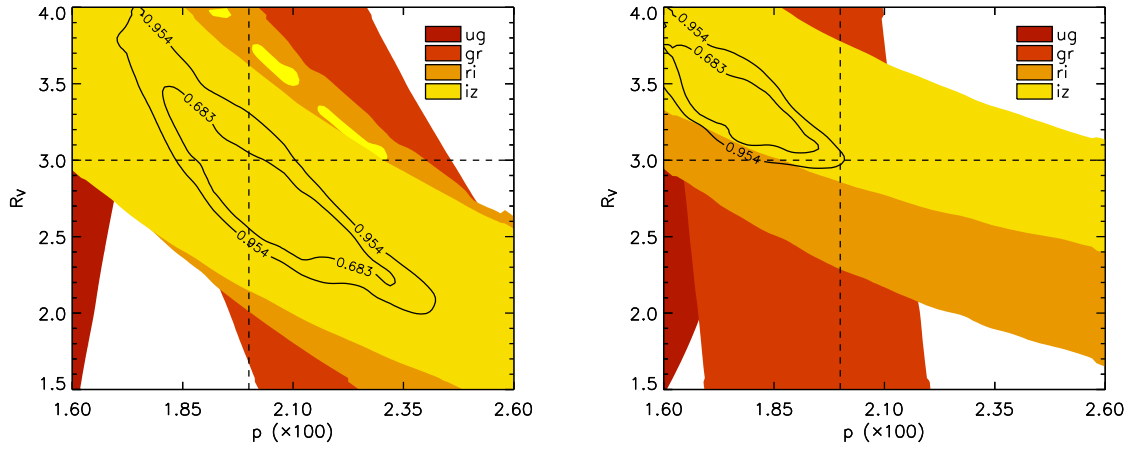


**Figure 9.** Constraints on  $p$  and  $R_V$  as derived from the observed colours of SDSS BCGs and the measured dust column density at the angular position of each BCG. Solid colours correspond 95.4% C.L. for two parameters. *Left:* Results for CCM dust corresponding to 95.4% C.L. for one parameter of  $p = 0.0205 \pm 0.0030$  and  $R_V = 2.89 \pm 0.88$ . *Right:* Results for Fitzpatrick dust corresponding to 95.4% C.L. for one parameter of  $p = 0.0177 \pm 0.0020$  and  $R_V = 3.42 \pm 0.48$ .

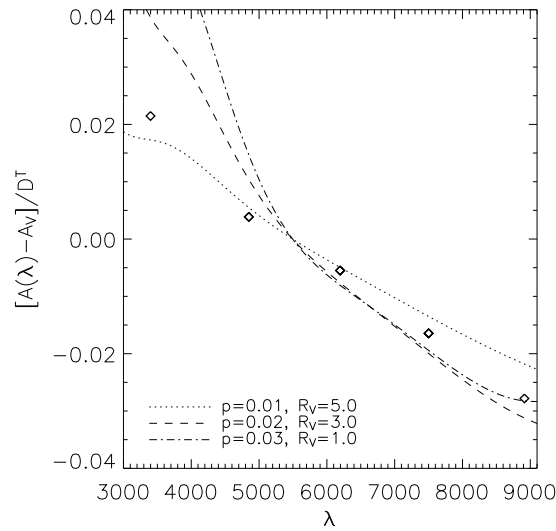


**Figure 10.** Empirical dust law as derived from BCG colours (diamonds) compared to the extinction curves of CCM dust with  $p = 0.01, R_V = 5.0$  (dotted curve),  $p = 0.02, R_V = 3.0$  (dashed curve) and  $p = 0.03, R_V = 1.0$  (dash-dotted curve).

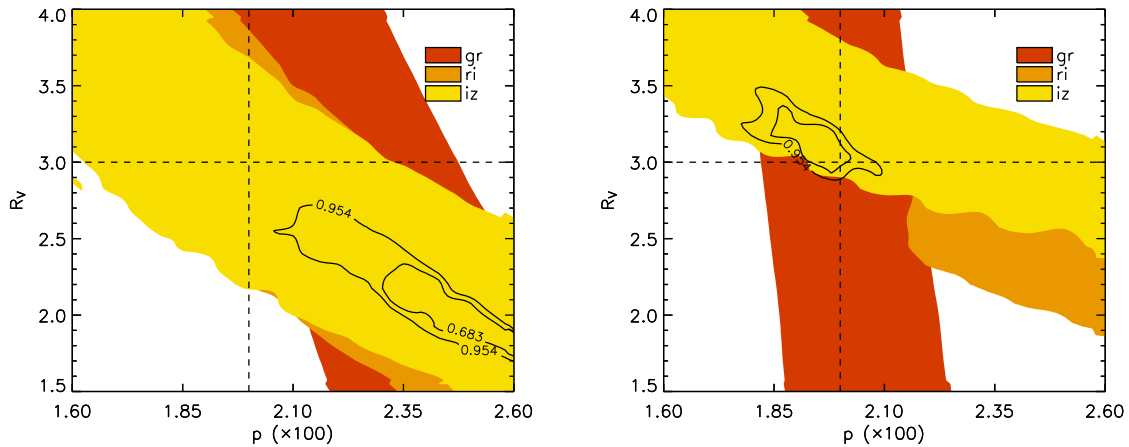


**Figure 11.** Constraints on  $p$  and  $R_V$  as derived from the observed colours of SDSS LRGs and the measured dust column density at the angular position of each LRG. Solid colours correspond 95.4% C.L. for two parameters. *Left:* Results for CCM dust corresponding to 95.4% C.L. for one parameter of  $p = 0.026 \pm 0.004$  and  $R_V = 1.95 \pm 0.35$ . *Right:* Results for Fitzpatrick dust corresponding to 95.4% C.L. for one parameter of  $p = 0.019 \pm 0.0025$  and  $R_V = 3.16 \pm 0.36$ .

## 6. Large Red Galaxies

Since Large Red Galaxies (LRGs) are also known to be homogeneous in terms of colours, we have extracted data for 114151 LRGs from the SDSS data base. Generally, all colours involving the  $u$ -band are not well-determined. Typically, we have (at  $z \sim 0.3$ ):  $\sigma(u - g) = 0.84$ ,  $\sigma(g - r) = 0.086$ ,  $\sigma(r - i) = 0.043$  and  $\sigma(i - z) = 0.056$ . We therefore do not use any colours involving the  $u$ -band in this analysis. Fitting for  $p$  and  $R_V$  gives the results shown in Fig. 11. Our constraints are  $p = 0.026 \pm 0.004$  and  $R_V = 1.95 \pm 0.35$  (CCM) and  $p = 0.019 \pm 0.0025$  and  $R_V = 3.16 \pm 0.36$  (FTZ) (95.4% C.L. for one parameter). Compared to the QSO and BCG analysis, the absence of the  $u$ -band pushes best fit values towards higher  $p$  and lower  $R_V$ . Assuming  $R_V = 3$ , compared to  $r - i$  and  $i - z$  that gives  $p = 0.02$ , we have more extinction in  $g - r$  for the CCM parametrisation. For Fitzpatrick dust,  $r - i$  gives  $p = 0.02$  while  $g - r$  and  $i - z$  have more extinction. In Fig. 12, we show the derived dust law.

## 7. Discussion

As seen in the previous sections, there are slight differences in the preferred values of  $p$  and  $R_V$ , depending on the dust parametrisation and the data set used. Generally, for the CCM parametrisation with  $R_V = 3$ , for  $r - i$  and  $i - z$ , we get  $p = 0.02$ . We have more extinction (higher  $p$ ) in  $g - r$  and less in  $u - g$ . For Fitzpatrick dust,  $r - i$  gives  $p = 0.02$  while  $g - r$  and  $i - z$  have more extinction and  $u - g$  less. How can we understand these differences? First, we need to understand the difference between the

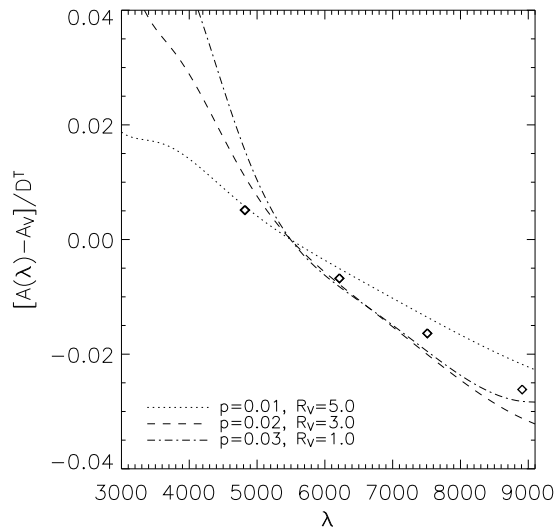


**Figure 12.** Empirical dust law as derived from LRG colours (diamonds) compared to the extinction curves of CCM dust with  $p = 0.01, R_V = 5.0$  (dotted curve),  $p = 0.02, R_V = 3.0$  (dashed curve) and  $p = 0.03, R_V = 1.0$  (dash-dotted curve).

CCM and FTZ dust extinction parametrisations. In Fig. 13, we plot

$$\frac{f(\lambda)_{FTZ} - f(\lambda)_{CCM}}{f(\lambda)_{CCM}}. \quad (8)$$

The reason that we need higher  $p$  for  $i - z$  for the FTZ model is that the extinction curve is flatter there compared to the CCM case. We also see that it is steeper for  $g - r$  which means that we get a lower  $p$  for that colour. That is, we need a dust law that is slightly steeper between for  $g - r$  and flatter for  $u - g$  compared to CCM. As for differences between the data sets, comparing BCGs and LRGs, we see that the differences can be explained by having a flatter template spectrum for LRGs in the region covering  $g - r$ , compared to the BCG template. Comparing BCGs and QSOs, differences can be resolved by either having the BCG template flatter for  $u - g$  and  $g - r$ , or the QSO template steeper in the same wavelength region.

## 8. $R_V$ -variations

It is not unreasonable to assume that the distributions of grain sizes, and thus also the resulting value of  $R_V$ , is different in high and low density environments. Whether grains are generally larger or smaller in high density environments depend on whether grain-grain collisions are more likely to cause coalescence or shattering. We therefore check for any evidence for correlations between  $R_V$  and the dust column density by dividing our sample into subsamples with different column densities. Note however that a high column density not necessarily corresponds to a high physical density. In Fig. 14, we show constraints from dividing the QSO sample into two regions with low ( $D^T < 3$  MJy

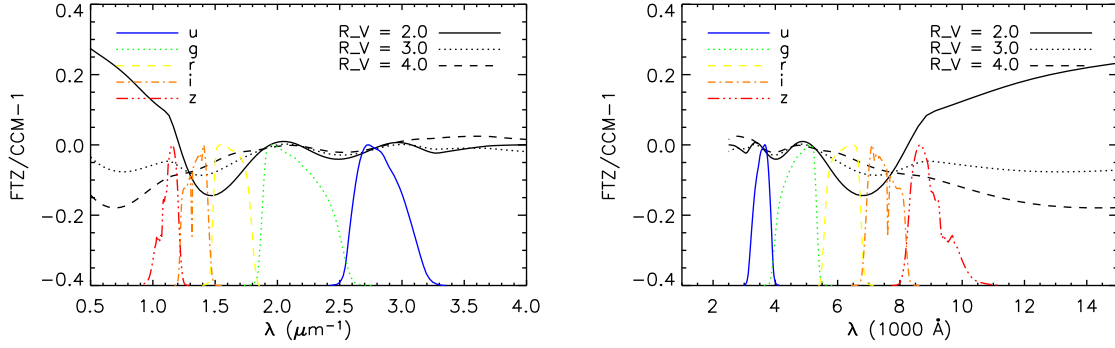


**Figure 13.** The difference between the CCM and FTZ dust extinction curves.

$\text{sr}^{-1}$ ) and high ( $D^T > 3 \text{ MJy sr}^{-1}$ ) dust column density. Our constraints for CCM are  $p = 0.020 \pm 0.0016$  and  $R_V = 3.06 \pm 0.56$  ( $D^T < 3 \text{ MJy sr}^{-1}$ ) and  $p = 0.019 \pm 0.0019$  and  $R_V = 3.09 \pm 0.65$  ( $D^T > 3 \text{ MJy sr}^{-1}$ ). For Fitzpatrick dust,  $p = 0.019 \pm 0.0016$  and  $R_V = 3.28 \pm 0.37$  ( $D^T < 3 \text{ MJy sr}^{-1}$ ) and  $p = 0.018 \pm 0.0018$  and  $R_V = 3.23 \pm 0.41$  ( $D^T > 3 \text{ MJy sr}^{-1}$ ) (95.4% C.L. for one parameter). This simple test does not provide evidence for any correlation between the dust column density and dust properties.

### 8.1. $\sigma(R_V)$ and $\sigma(A_V)$

If dust has spatially varying properties, depending on the size of the regions, we would expect the colour dispersion to be bigger behind regions with high column density  $D^T$ , in addition to being redder. For filters  $X$  and  $Y$ , we can write the colour  $E(X - Y)$  as a combination of the intrinsic colour  $E_i(X - Y)$  and the dust induced colour  $E_d(X - Y)$ ,

$$E(X - Y) = E_i(X - Y) + E_d(X - Y), \quad (9)$$

and the corresponding colour dispersion

$$\sigma[E(X - Y)]^2 = \sigma[E_i(X - Y)]^2 + \sigma[E_d(X - Y)]^2, \quad (10)$$

where

$$E_d(X - Y) = \left( \frac{A_X}{A_V} - \frac{A_Y}{A_V} \right) A_V \equiv f_{XY}(R_V) A_V, \quad (11)$$

and

$$\begin{aligned} \sigma[E_d(X - Y)]^2 &= \left[ \left( \frac{R_V}{f_{XY}} \frac{\partial f_{XY}}{\partial R_V} \right)^2 \left( \frac{\sigma_{R_V}}{R_V} \right)^2 + \left( \frac{\sigma_{A_V}}{A_V} \right)^2 \right] E_d(X - Y)^2 \\ &\equiv g[X, Y, R_V, \sigma(R_V), \sigma(A_V)] E_d(X - Y)^2. \end{aligned} \quad (12)$$

In Fig. 15, we plot the variance  $\sigma[E(X - Y)]^2$  as a function of  $E_d(X - Y)^2$  for each standard colour of the QSO sample, expecting the variance at zero  $E_d(X - Y)^2$  to give the intrinsic colour variance  $\sigma[E_i(X - Y)]^2$  and the slope to be related to the scatter in  $R_V$  and  $A_V$  through the function  $g[X, Y, R_V, \sigma(R_V), \sigma(A_V)]$  (using the CCM dust

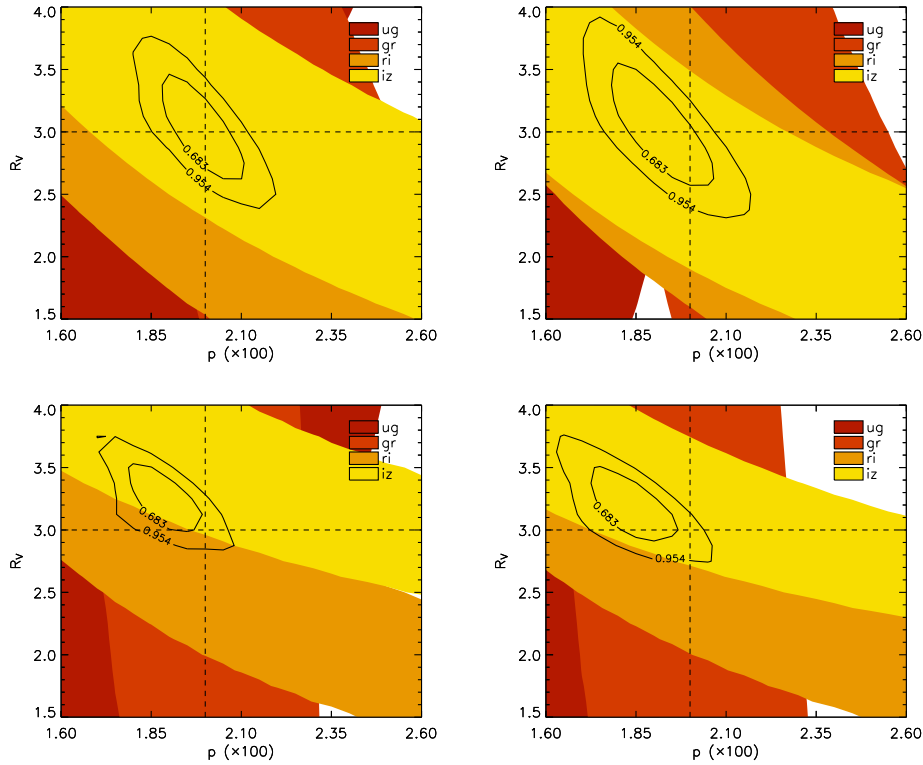


**Figure 14.** Constraints on  $p$  and  $R_V$  when dividing data into regions with low ( $D^T < 3$  MJy sr $^{-1}$ ) and high ( $D^T > 3$  MJy sr $^{-1}$ ) dust column density. There is no evidence for any correlation between the dust column density and dust properties. *Upper left:* Results for CCM dust for all regions with  $D^T < 3$  MJy sr $^{-1}$  corresponding to 95.4% C.L. for one parameter of  $p = 0.020 \pm 0.0016$  and  $R_V = 3.06 \pm 0.56$ . *Upper right:* Results for CCM dust at  $D^T > 3$  MJy sr $^{-1}$  giving  $p = 0.019 \pm 0.0019$  and  $R_V = 3.09 \pm 0.65$ . *Lower left:* Results for Fitzpatrick dust at  $D^T < 3$  MJy sr $^{-1}$  giving  $p = 0.019 \pm 0.0016$  and  $R_V = 3.28 \pm 0.37$ . *Lower right:* Results for Fitzpatrick dust at  $D^T > 3$  MJy sr $^{-1}$  giving  $p = 0.018 \pm 0.0018$  and  $R_V = 3.23 \pm 0.41$ .

extinction parametrisation). As can be seen, there are no obvious correlations between  $\sigma[E(X - Y)]^2$  and  $E_d(X - Y)^2$  (or equivalently the dust column density  $D^T$ ). Assuming  $\sigma_{R_V}/R_V$  and  $\sigma_{A_V}/A_V$  to be constant (although the results depicted in Fig. 15 indicate that this assumption may be too simplistic), we can constrain their values from the fitted straight line slopes. Results from such an analysis are shown in Fig. 16. The bluer colours show no increase in the colour variance with dust column density, whereas  $i - z$  show a slight increase in the variance indicating a possible variance in  $\sigma_{A_V}/A_V$  at the 30% level. This said, there are a few caveats that should be remembered: First, this is under the assumption that the relation between the variance and the colour indeed is linear. Second, results for  $i - z$  are not consistent with the bluer colours that show no signs of a scatter in the dust properties (although it is possible that the scatter only manifests itself at longer wavelengths). Third, there is a (weak) binning dependence when calculating the dispersion as a function of  $E_d(X - Y)^2$ . To summarize, there is no

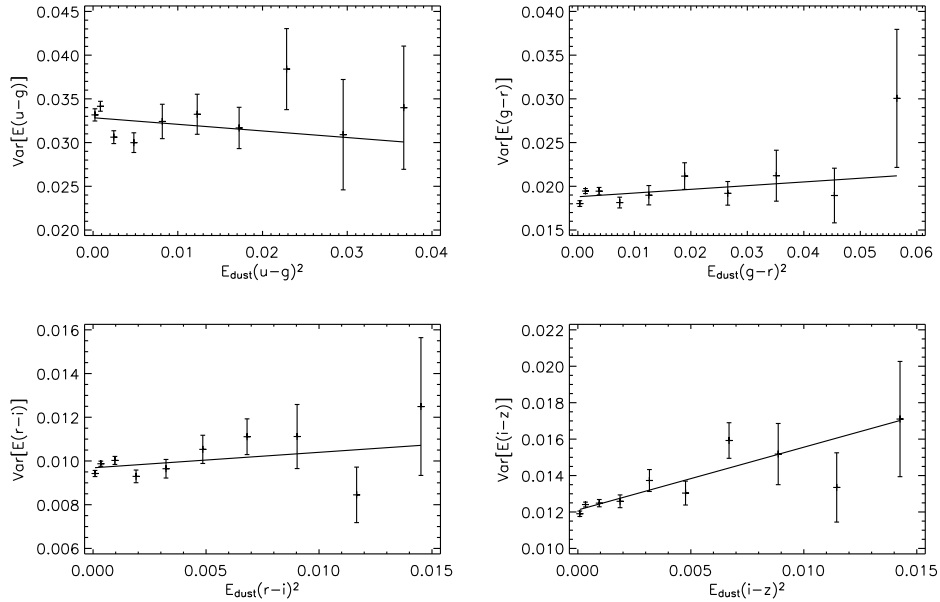


**Figure 15.** The variance  $\sigma[E(X - Y)]^2$  as a function of  $E_d(X - Y)^2$  for each standard colour of the QSO sample. The total variance at zero  $E_d(X - Y)^2$  is the intrinsic colour variance  $\sigma[E_i(X - Y)]^2$  and the slope is related to the scatter in  $R_V$  and  $A_V$ .

evidence in the QSO data for any additional scatter in the observed colours in regions with high column density, indicating that dust properties are relatively homogeneous averaged over the size of spatial regions probed in this paper, except perhaps for a hint of such an increased scatter at the reddest optical wavelengths probed by the QSO data.

## 9. Summary

By investigating the correlations between dust column density as inferred from infrared data and the observed colours of celestial objects at cosmological distances with small colour dispersion, we constrain the properties of Milky Way dust. Results from QSOs, BCGs and LRGs colours are broadly consistent, indicating a proportionality constant between the reddening  $E(B - V) \equiv A_B - A_V$  and the dust column density  $D^T$  (given in units of MJy/sr) of  $p = E(B - V)/D^T \sim 0.02$  and a reddening parameter  $R_V \equiv A_V/E(B - V) \sim 3$  with relative uncertainties of the order 10%. In spite of the increased statistics, the fractional error of  $p$  is similar to that of Schlegel et al. [12], the reason being that we simultaneously fit for  $R_V$  and that the uncertainty is dominated by the possibility of systematic shifts in the effective filter wavelengths.

The data does not provide any evidence for any dependence of the dust properties as a function of dust column density, neither for any sizable scatter in the dust properties on the scales probed by the data, except a hint of scatter  $\sigma_{A_V}/A_V \gtrsim 0.3$  in the extinction properties of dust at the longest wavelengths probed by the data (corresponding to  $i - z$ ). We have also checked that within the uncertainties, there is no evidence of

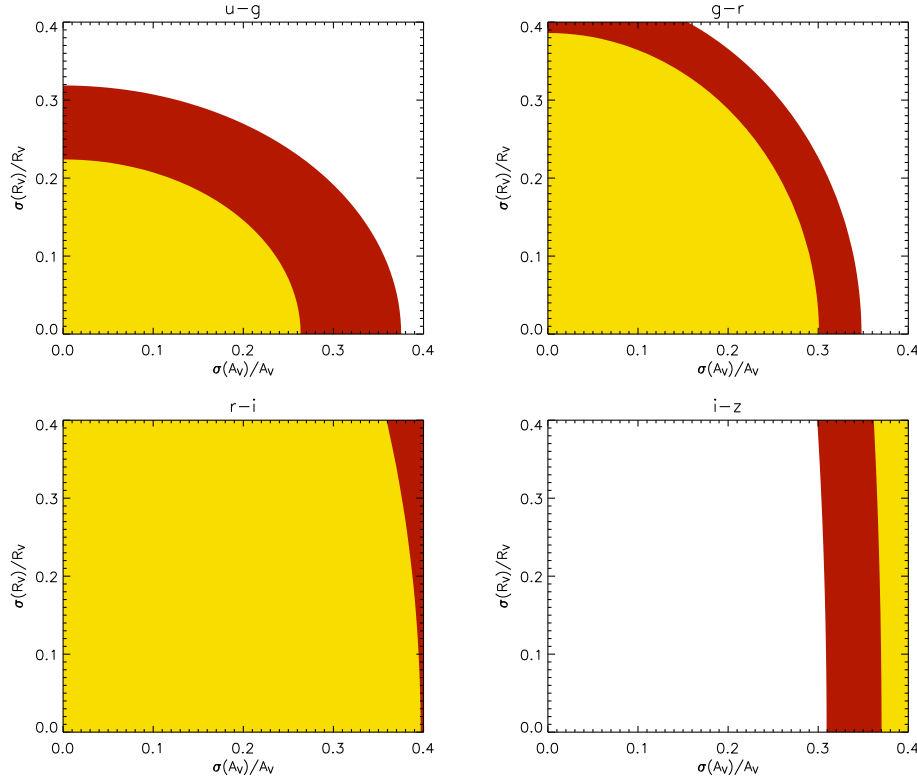


**Figure 16.** Constraints on constant  $\sigma_{R_V}/R_V$  and  $\sigma_{A_V}/A_V$  derived from the linear fits depicted in Fig. 15. The coloured regions correspond to 95.4% CL (red) and 68.3% CL (yellow), both for two parameters.

any systematic difference between the dust extinction properties in the northern and southern hemisphere. Assuming the dust maps of Schlegel et al. [12] to be correct, it is thus fair to assume that we can correct for Milky Way dust by applying a proportionality constant  $p = E(B - V)/D^T \sim 0.02$  with reddening parameter  $R_V \sim 3$  to the dust maps, in accordance with the results of Schlegel et al. [12].

## References

- [1] Berry, M., Ž. Ivezić, B. Sesar, et al., 2011, ArXiv e-prints
- [2] Cardelli, J. A., G. C. Clayton, and J. S. Mathis, 1989, *Astrophys. J.*, 345, 245
- [3] Doi, M., M. Tanaka, M. Fukugita, et al., 2010, *Astron. J.*, 139, 1628
- [4] Fitzpatrick, E. L., 1999, *The Publications of the Astronomical Society of the Pacific*, 111, 63
- [5] Koester, B. P., T. A. McKay, J. Annis, et al., 2007, *Astrophys. J.*, 660, 239
- [6] Kohyama, T., H. Shibai, M. Fukagawa, and Y. Hibi, 2010, *Astrophys. J.*, 719, 873
- [7] Östman, L., A. Goobar, and E. Mörtzell, 2006, *Astron. Astrophys.*, 450, 971
- [8] Östman, L., A. Goobar, and E. Mörtzell, 2008, *Astron. Astrophys.*, 485, 403



- [9] Östman, L. and E. Mörtzell, 2005, *Journal of Cosmology and Astroparticle Physics*, 2, 5
- [10] Peek, J. E. G. and G. J. Graves, 2010, *Astrophys. J.*, 719, 415
- [11] Richards, G. T., X. Fan, H. J. Newberg, et al., 2002, *Astron. J.*, 123, 2945
- [12] Schlegel, D. J., D. P. Finkbeiner, and M. Davis, 1998, *Astrophys. J.*, 500, 525
- [13] Schneider, D. P., P. B. Hall, G. T. Richards, et al., 2007, *Astron. J.*, 134, 102
- [14] Telfer, R. C., W. Zheng, G. A. Kriss, and A. F. Davidsen, 2002, *Astrophys. J.*, 565, 773
- [15] Vanden Berk, D. E., G. T. Richards, A. Bauer, et al., 2001, *Astron. J.*, 122, 549

## Acknowledgments

EM acknowledge support for this study by the Swedish Research Council. EM also acknowledges discussions with Brice Menard and Ariel Goobar.

Funding for the SDSS and SDSS-II has been provided by the Alfred P. Sloan Foundation, the Participating Institutions, the National Science Foundation, the US Department of Energy, the National Aeronautics and Space Administration, the Japanese Monbukagakusho, the Max Planck Society, and the Higher Education Funding Council for England. The SDSS is managed by the Astrophysical Research Consortium for the Participating Institutions. The Participating Institutions are the American Museum of Natural History, Astrophysical Institute Potsdam, University of Basel, Cambridge University, Case Western Reserve University, University of Chicago, Drexel University, Fermilab, the Institute for Advanced Study, the Japan Participation Group, Johns Hopkins University, the Joint Institute for Nuclear Astrophysics, the Kavli Institute for Particle Astrophysics and Cosmology, the Korean Scientist Group, the Chinese Academy of Sciences (LAMOST), Los Alamos National Laboratory, the Max-Planck-Institute for Astronomy (MPIA), the Max-Planck-Institute for Astrophysics (MPA), New Mexico State University, Ohio State University, University of Pittsburgh, University of Portsmouth, Princeton University, the United States Naval Observatory, and the University of Washington.